

# **Numerical modeling of shear-wave splitting and azimuthal velocity analysis in fractured media**

Zimin Zhang, Don C. Lawton, and Robert R. Stewart

## **ABSTRACT**

This report presents the processing and interpretation of seismic modeling data of the earth models for a fractured layer, based on well logs associated with potash mining. The purpose of the work is to study azimuthal seismic anisotropy, shear-wave splitting, and time-lapse seismic signals caused by vertically aligned cracks. The results show that seismic velocity anisotropy can be detected by both vertical and horizontal components of the HTI earth model; it is especially evident on radial component. Shear-wave splitting is evident and the crack orientation determined from the polarization of fast and slow shear waves is consistent with the input model. The time-shift and amplitude changes due to anisotropic layer are also apparent on both vertical and radial component data. The time-shift on radial data is up to 5ms and the amplitude change is up to 46%.

The modeled data correlate nicely with the well data. Considering the correlation results of well and surface seismic data in the previous study, this suggests that multi-component seismic data are interpretable in this potash area. This also suggests that by searching for seismic anisotropy, shear-wave splitting on the multi-component seismic data or by looking for changes in repeated seismic surveys, we may be able to detect/monitor cracks and crack orientation in HTI model.

## **INTRODUCTION**

### **Geology background and previous study**

A major problem for potash mining can be brine inflow. This may cause ore loss and operational problems. In the studied Saskatchewan potash mining area, potash ore (used as fertilizer and other products) is situated 20-30m from the top of a 100-200m thick salt unit (Figure 1), Prairie Evaporite Formation which is present through much of the Williston Basin region. Above the mining interval, there can be aquifers at the bottom of the Souris River Formation and upper part of the Dawson Bay (Figure 1). Between the aquifers and ore zone, the formation is composed of shale, dolomite and dolomitized limestone. All these rocks may be fractured and any fracturing of normally impermeable carbonate rocks could create a brine inflow path that might compromise potash mining operations.

An effective way to mitigate the risk posed by brine flows is to map and predict the volume and location of potentially affected areas prior to mining. To investigate the feasibility of using multi-component and repeated (time-lapse) seismic methods for crack mapping and monitoring, rock-physics modeling and synthetic seismogram were used to predict seismic velocity changes and seismic signatures of cracks in the Dawson Bay formation (Zhang and Stewart, 2008). The results indicate that P-wave and S-wave velocities will decrease (often significantly) with cracks or fractures. Vertically aligned cracks may also display azimuthal anisotropy. Synthetic seismograms calculated using

the original well logs and those with cracks show observable changes such as “push-down” effects or time lags and amplitude variations with offset.

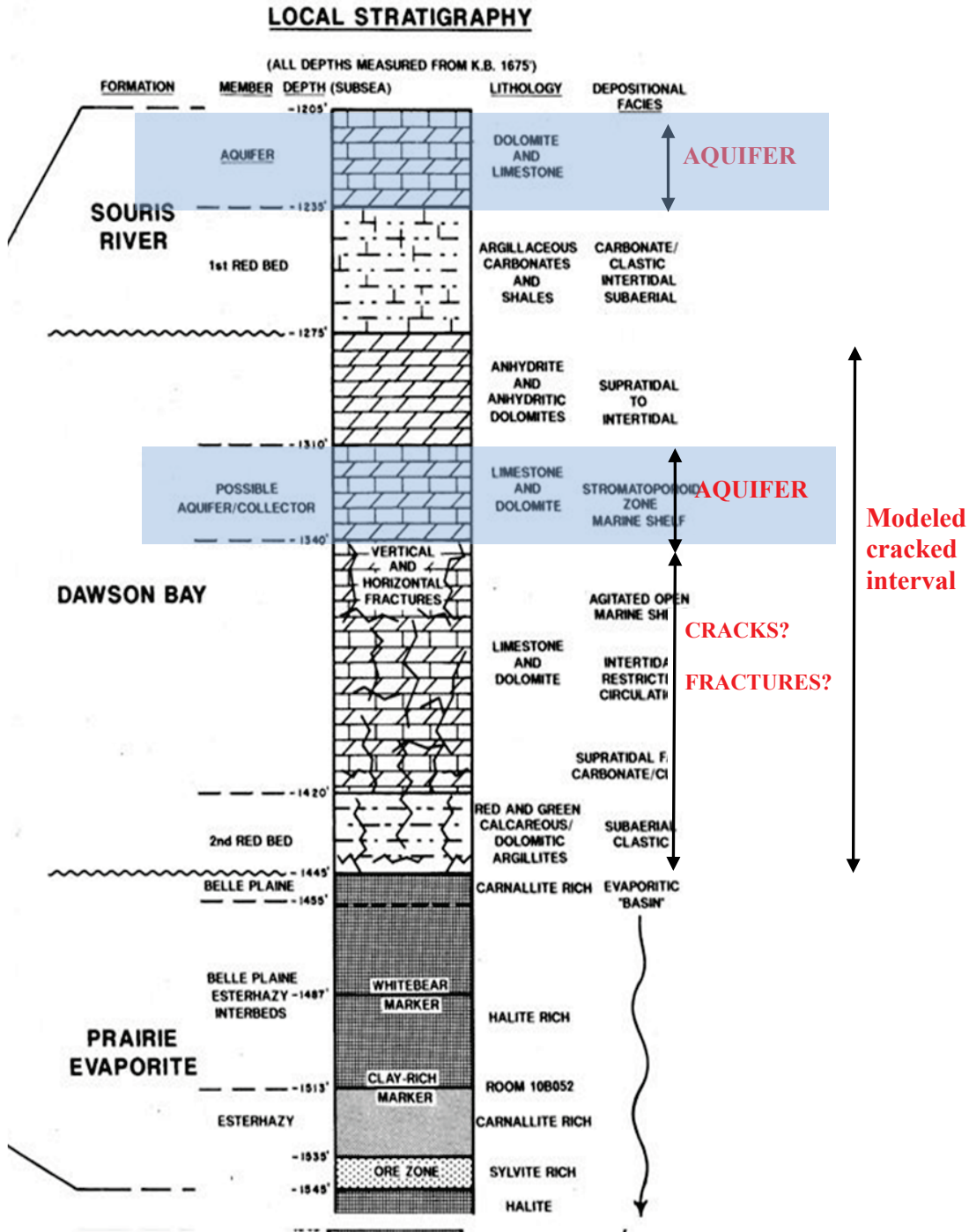


Figure 1. Local stratigraphy of Prairie Evaporite and overlying formations in the mining area. The Dawson Bay carbonates, dolomites, and shales can host fractures (from R. Edgecombe, personal communication, 2008).

Since the synthetic seismogram modeling program in the previous study is for isotropic velocities, seismic signatures of anisotropy caused by aligned cracks can not be seen. In this report, seismic modeling data for uncracked (isotropic) and cracked (anisotropic) earth models are used for shear-wave splitting, seismic velocity anisotropy, and time lapse seismic signature analysis.

## Acquisition of 3D-3C seismic modeling data

### *Input earth models*

Two laterally homogeneous earth models were input for 3D-3C seismic modeling. The uncracked earth model was built from the blocked well logs at the study area. By replacing rock properties of the full Dawson Bay Formation by the rock physics modeling results of vertically aligned cracks formation, an anisotropic (HTI) earth model was created for seismic modeling.

Figure 2 show the general stratigraphic chart and blocked well logs for the density and velocity models. The shallow parts are shales and sandstones of Cretaceous and Triassic age. The Devonian strata are mainly carbonates with two evaporite formations: Davidson Evaporite and Prairie Evaporite. Underlying the Prairie Evaporite is the Winnipegosis carbonate. The red rectangle denotes the location of cracked layer, the Dawson Bay Formation. The upper part of it is mostly dolomite or dolomitized limestone, the lower part is the Second Red Bed shale. The rock properties for the Dawson Bay Formation are listed in Table 1.

Figure 3 shows the interval velocity models of P-wave and shear-wave for numerical modeling. The layered models are created based on the blocked well logs. The maximum measured depth of well logs is 1378.2m. The velocities at deeper locations than this depth are set to be equal to the velocities at 1378.2m.

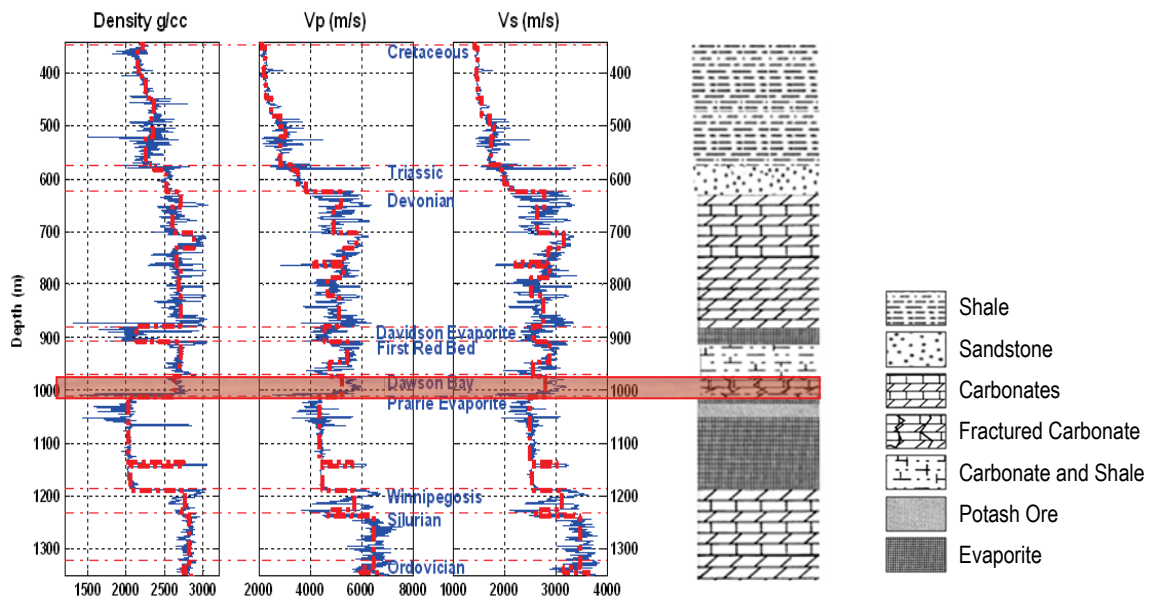


Figure 2. Stratigraphy chart (modified after Fuzesy, 1982) and blocked well logs. The red rectangle denotes the location of modeled HTI layer.

Table 1. Rock properties of the Dawson Bay, the values are averaged over the formation (coordinate used for stiffness matrix: x1 - normal direction of crack plane (horizontal); x3 - vertical direction).

Top	970.8 m						
Thickness	40.4 m						
Crack parameters	1% penny-shape cracks, filled by brine with Vp 1430m/s, density 1100 kg/m <sup>3</sup> .						
	cracked			uncracked			
Density	2603.9 kg/m <sup>3</sup>			2630.2 kg/ m <sup>3</sup>			
Stiffness matrix (x10 <sup>10</sup> kg/m <sup>2</sup> ·s)	5.610	2.354	2.354	0	0	0	Vp: 5184.7 m/s Vs: 2792.9 m/s
	2.354	6.813	2.710	0	0	0	
	2.354	2.710	6.813	0	0	0	
	0	0	0	2.052	0	0	
	0	0	0	0	1.243	0	
	0	0	0	0	0	1.243	

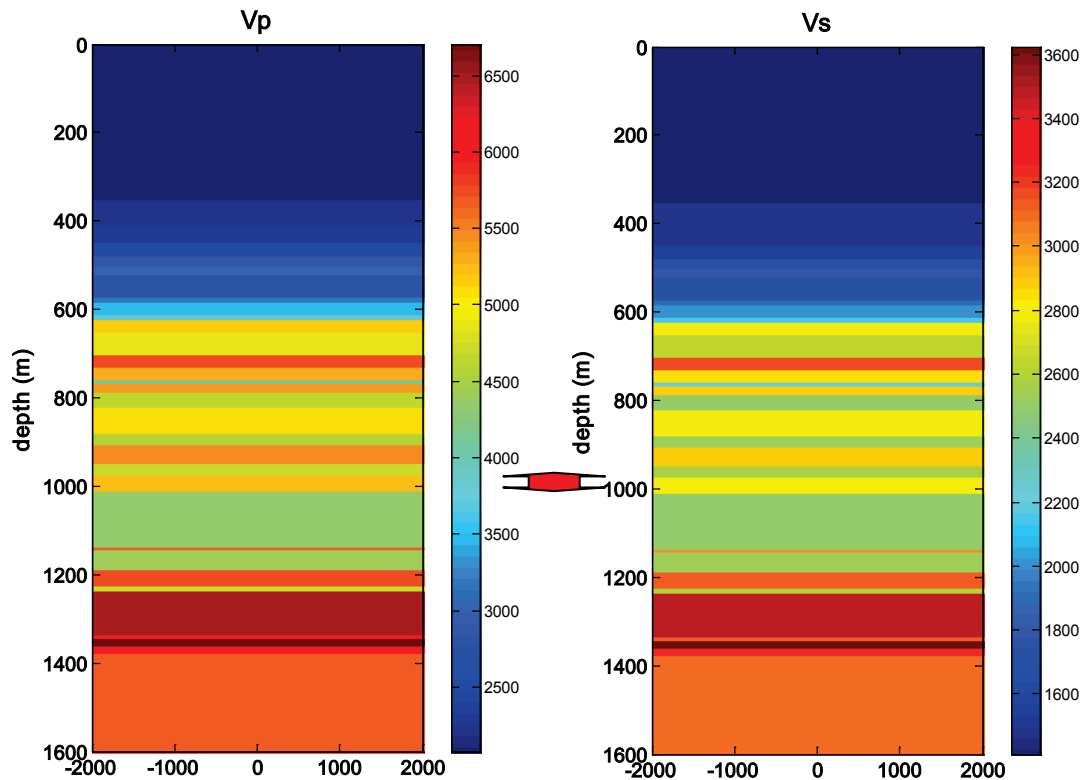


Figure 3. Input interval P-wave and shear-wave velocity layered models for numerical modeling. The HTI models are the same as isotropic model except for replacing the rock properties of Dawson Bay Formation by values with vertically aligned cracks. The anisotropic layer (Dawson Bay Formation) location is denoted by red arrow.

*Survey design and raw data analysis*

An exhaustive wide azimuth survey was designed for shear-wave splitting and seismic velocity anisotropy analysis (Figure 4); the parameters of the survey are shown in Table 2. Since the earth models are laterally homogeneous, only one shot was modeled with the source location at the center of the survey. The recording coordinate used is denoted by blue in Figure 4. X is in the direction normal to the fracture plane (isotropy axis). Y is along the fracture plane (isotropy plane). The seismic modeling uses frequency-wavenumber method. 3-C data sets were modeled for both isotropic and anisotropic models.

Table 2. Survey design parameters for numerical modeling

Survey size	4km x 4km
Receiver spacing	20 m
Receiver line spacing	20 m
Sample rate	2 ms
Record length	2048 ms
Source	Dynamite at the surface
Modeling frequency range	2 – 110 HZ

Figure 5 displays azimuth and offset distribution of the survey. The offset ranges from 0 to 2824 meters. The azimuth is from 0 to 360 degrees. The number of offsets for each azimuth is relatively even with some variation, and is suitable for the shear-wave splitting and velocity anisotropy analysis described later in this report.

Figure 6 and Figure 7 show the 3-component seismic data at the selected azimuth, 0°, 45°, 90°, and 135° (negative offsets at 180°, 225°, 270°, and 315° were combined respectively) for the isotropic model and anisotropic model respectively. The data quality is very good. In the recording coordinates, x-component receives no signal at 0° and 180°, while y-component has no signal at 90° and 270° for both isotropic and anisotropic earth models. Since there is no low velocity layer at the near surface, there is P wave and shear-wave leakage on horizontal components and the vertical component respectively. Amplitude spectra were also calculated for x, y, and z components of isotropic model (Figure 8), the frequency ranges are quite similar for all the three components, about 10-120 Hz.

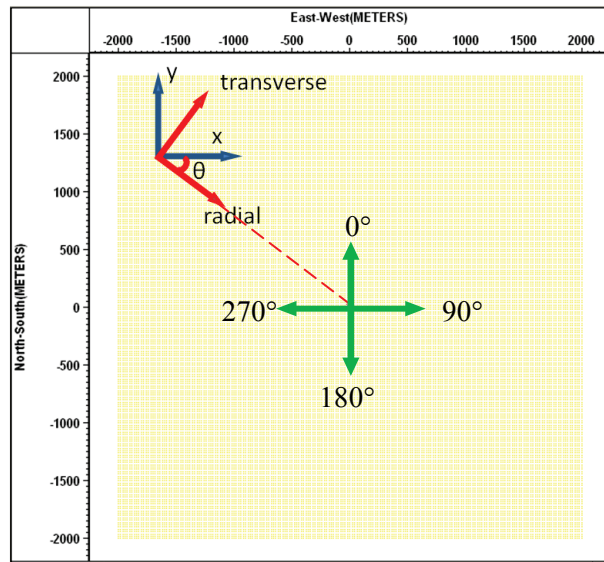


Figure 4. Schematic plot for coordinate system used for data recording and processing. The horizontal components were originally recorded in X & Y directions, for processing, the 2 components should be reoriented to radial and transverse directions. The source location is at the survey centre, red dash line denotes the direction from receiver point to source point. Azimuth used in processing is denoted by the green cross.

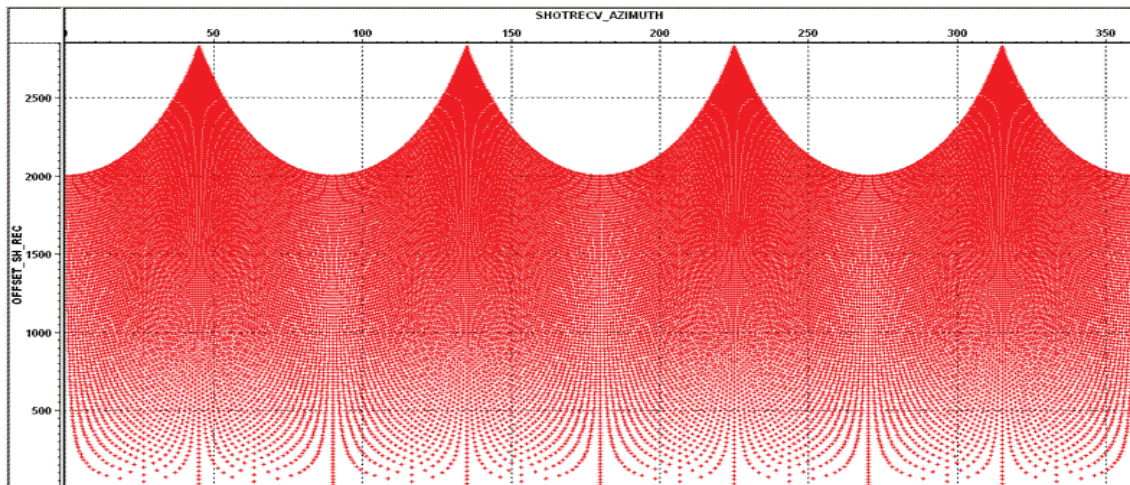


Figure 5. Azimuth and offset distribution of the survey.

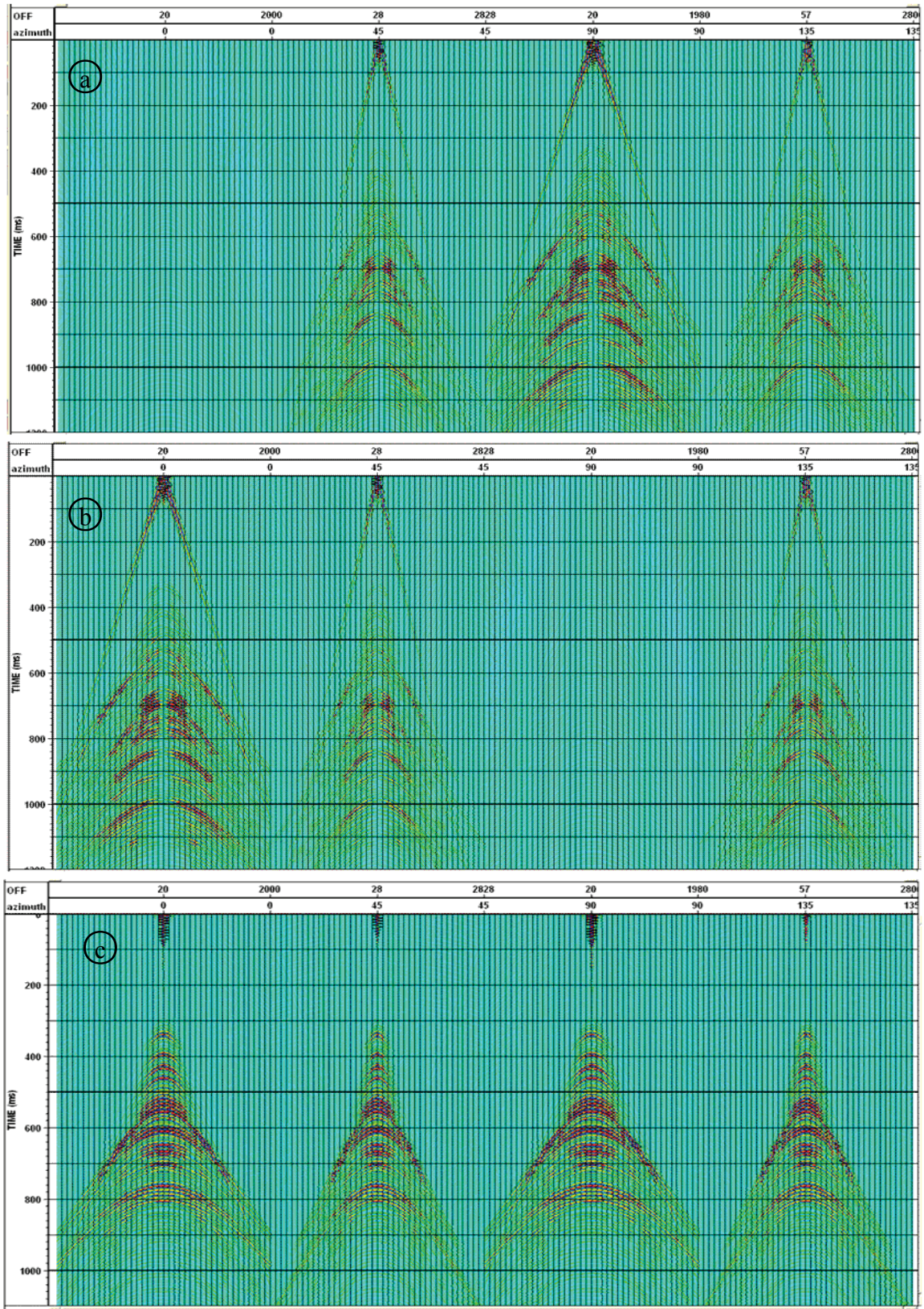


Figure 6. X, Y & Z components of isotropic earth model at azimuth 0°, 45°, 90°, and 135° (negative offsets at 180°, 225°, 270°, and 315° were combined respectively).

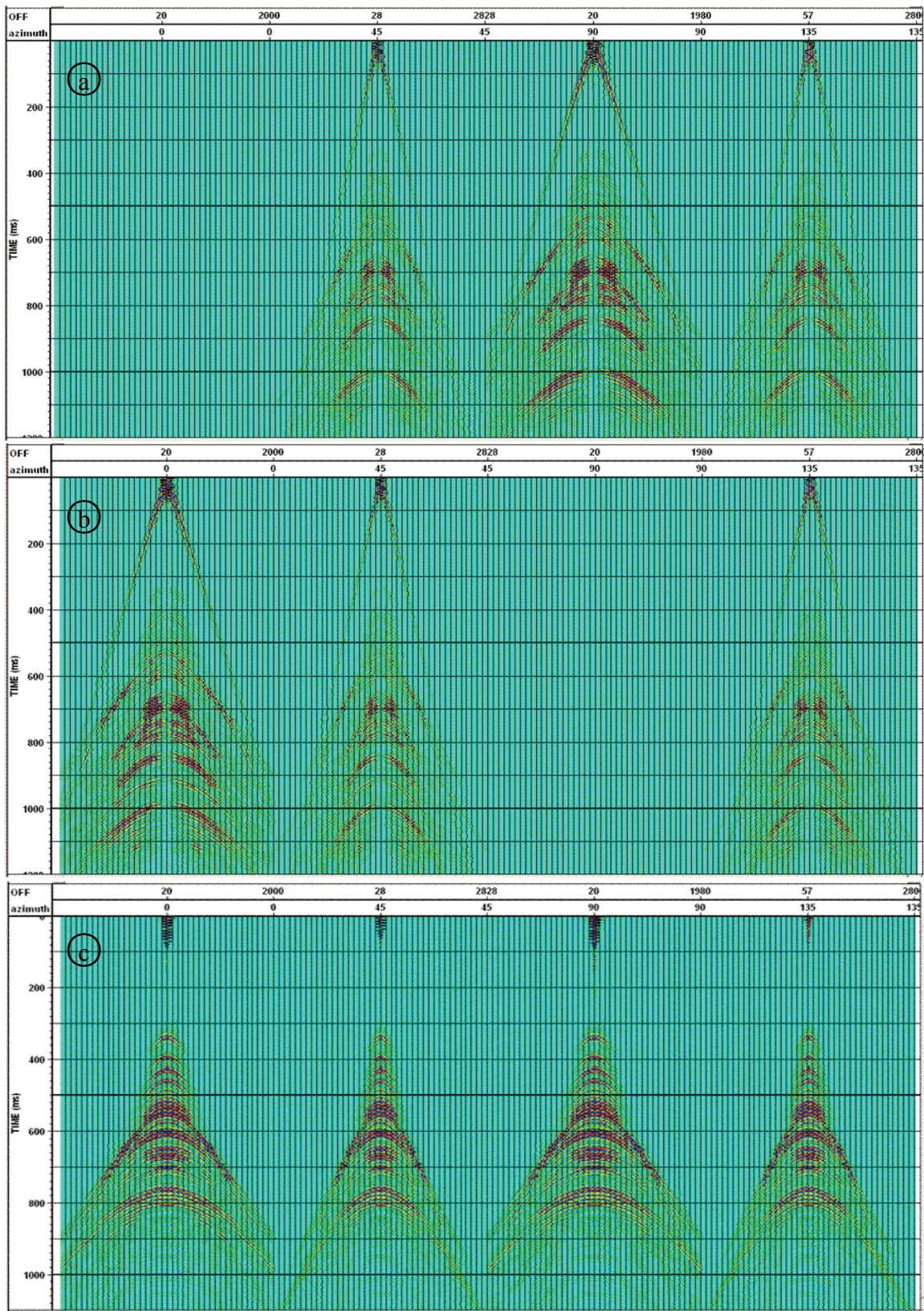


Figure 7. X, Y & Z components of anisotropic earth model at azimuth 0°, 45°, 90°, 135° (negative offsets at 180°, 225°, 270°, and 315° were combined respectively).

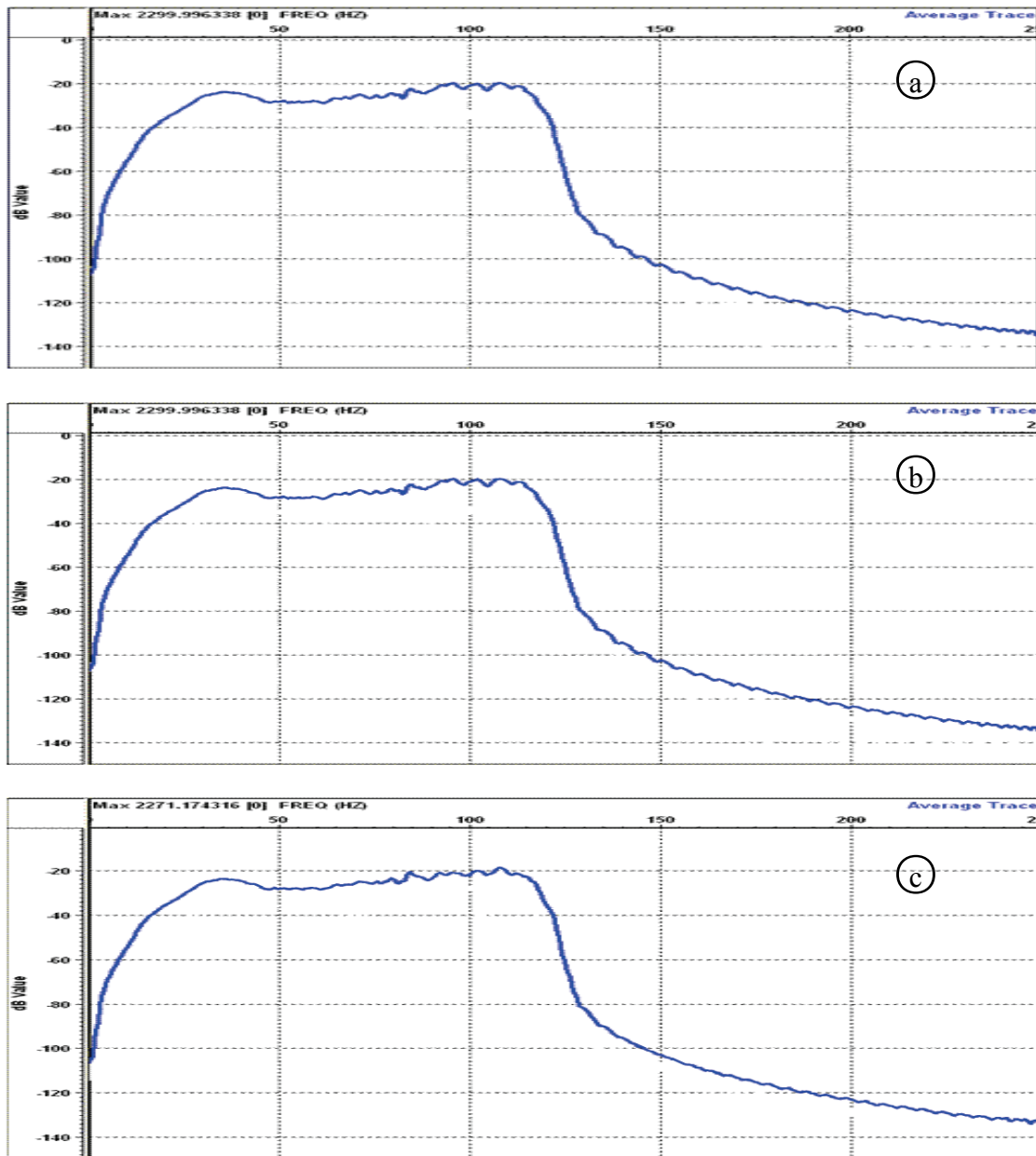


Figure 8. X, Y & Z components amplitude spectrum of isotropic earth model.

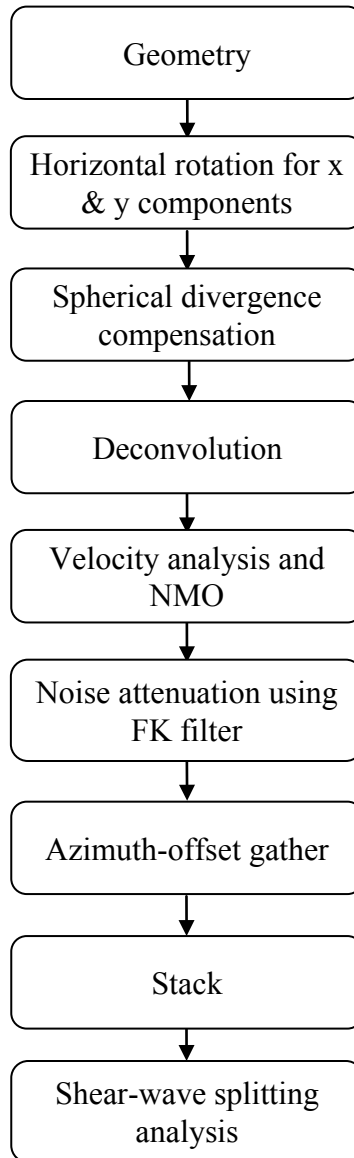
### SEISMIC DATA PROCESSING

Table 3 shows the seismic processing workflow used for shear-wave splitting analysis. Firstly, the geometry information, including source receiver locations, processing grid bin size, azimuth etc., were loaded for all the data sets.

Since the original horizontal components were recorded at x, y direction, they were reoriented to radial and transverse directions prior to other processing steps (denoted as red arrows in Figure 4). Figure 9 and Figure 11 display the horizontal rotation results for isotropic and HTI earth model data. As shown in Figure 9, for isotropic earth model, the shear wave energy is recorded in radial direction (SV wave). On transverse component,

no shear wave (SH wave) energy is found. For the HTI earth model, except for the dominant SV wave recorded in radial component, SH wave is also found below cracked layer location (about 850ms) on the transverse component except azimuths  $0^\circ$  and  $90^\circ$  (Figure 11). Figure 10 also displays polarity change of horizontal component between original recording coordination and rotated coordinates. On the x-component of x-direction receiver line across the source location, the polarity reverses across zero offset for both direct arrival and reflections. After horizontal rotation, the polarity is consistent across the source location on radial component for both wave types.

Table 3. 3C seismic data processing workflow for shear-wave splitting analysis.



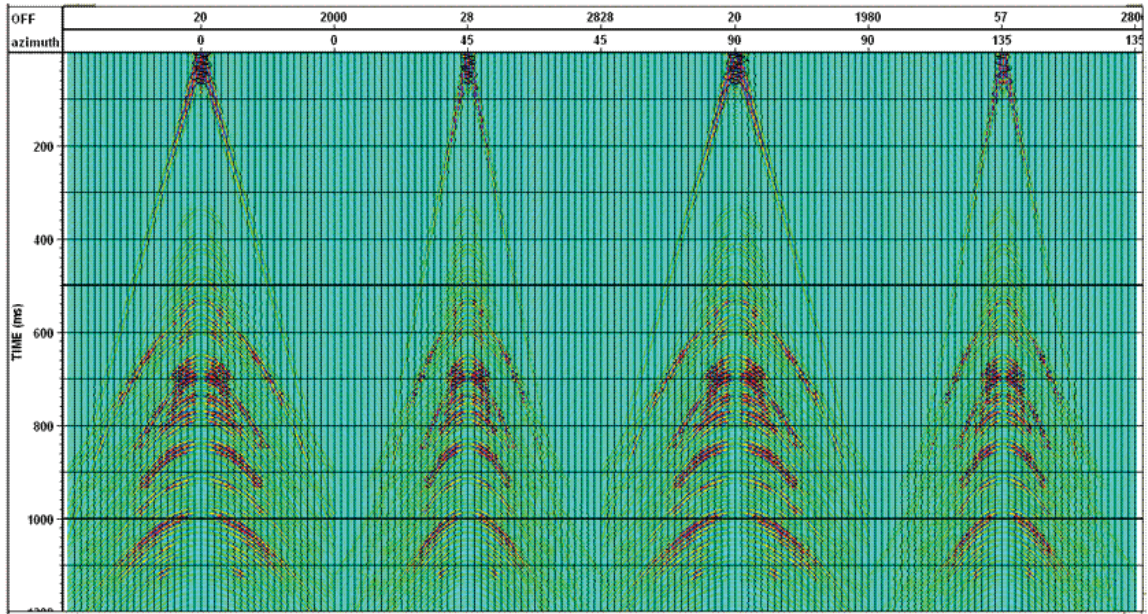


Figure 9. Radial component of isotropic earth model from horizontal rotation of X, Y components (at azimuth  $0^\circ$ ,  $45^\circ$ ,  $90^\circ$ ,  $135^\circ$ ). For laterally homogeneous isotropic media, transverse component receives no energy.

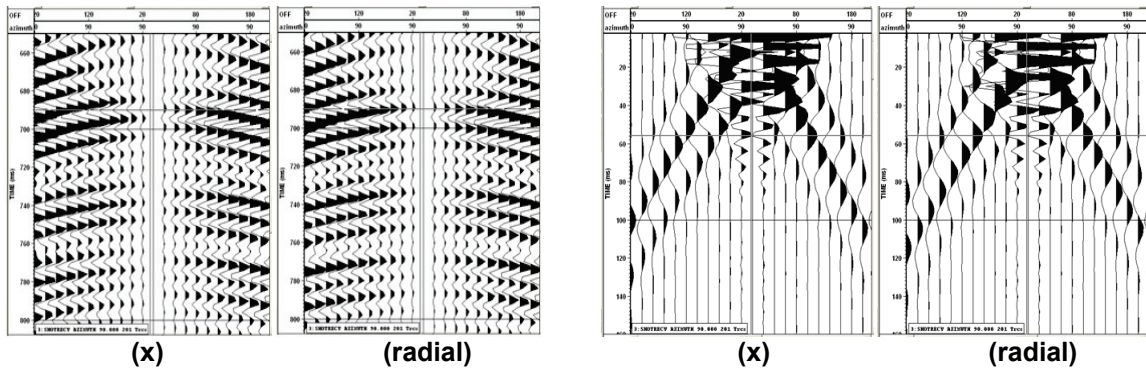


Figure 10. Comparison of reflection (left) and direct arrival (right) between x-component and radial component from horizontal rotation of isotropic earth model (at azimuth  $90^\circ$ ), note the polarity difference between the two data sets.

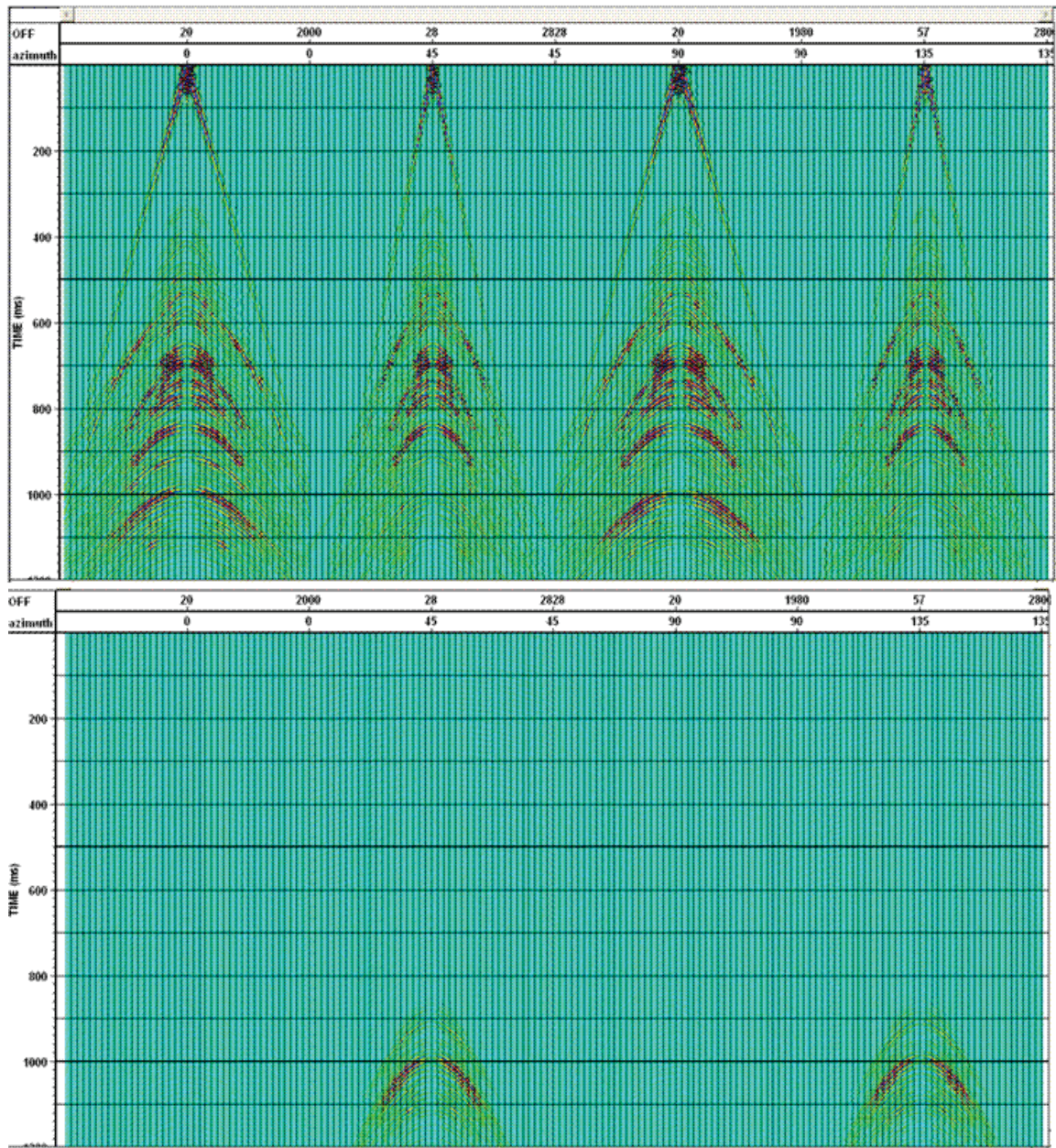


Figure 11. Radial (top) and transverse (bottom) components of HTI earth model from horizontal rotation of X, Y components (at azimuth 0°, 45°, 90°, 135°).

Spherical divergence was corrected by PP and PS velocities for vertical and horizontal components respectively. Zero-phase deconvolution was then applied to the data. Figure 12 shows the comparisons of vertical component gather, autocorrelation function and amplitude spectrum at azimuth 0° before and after deconvolution of the data from the isotropic model. After deconvolution, the reflection character is clearer (Figure 12). From the autocorrelation function of the data, we can see that the wavelet sidelobes are suppressed and lateral coherency is improved by deconvolution. The frequency spectrum is also flattened and is more spatially coherent (Figure 12).

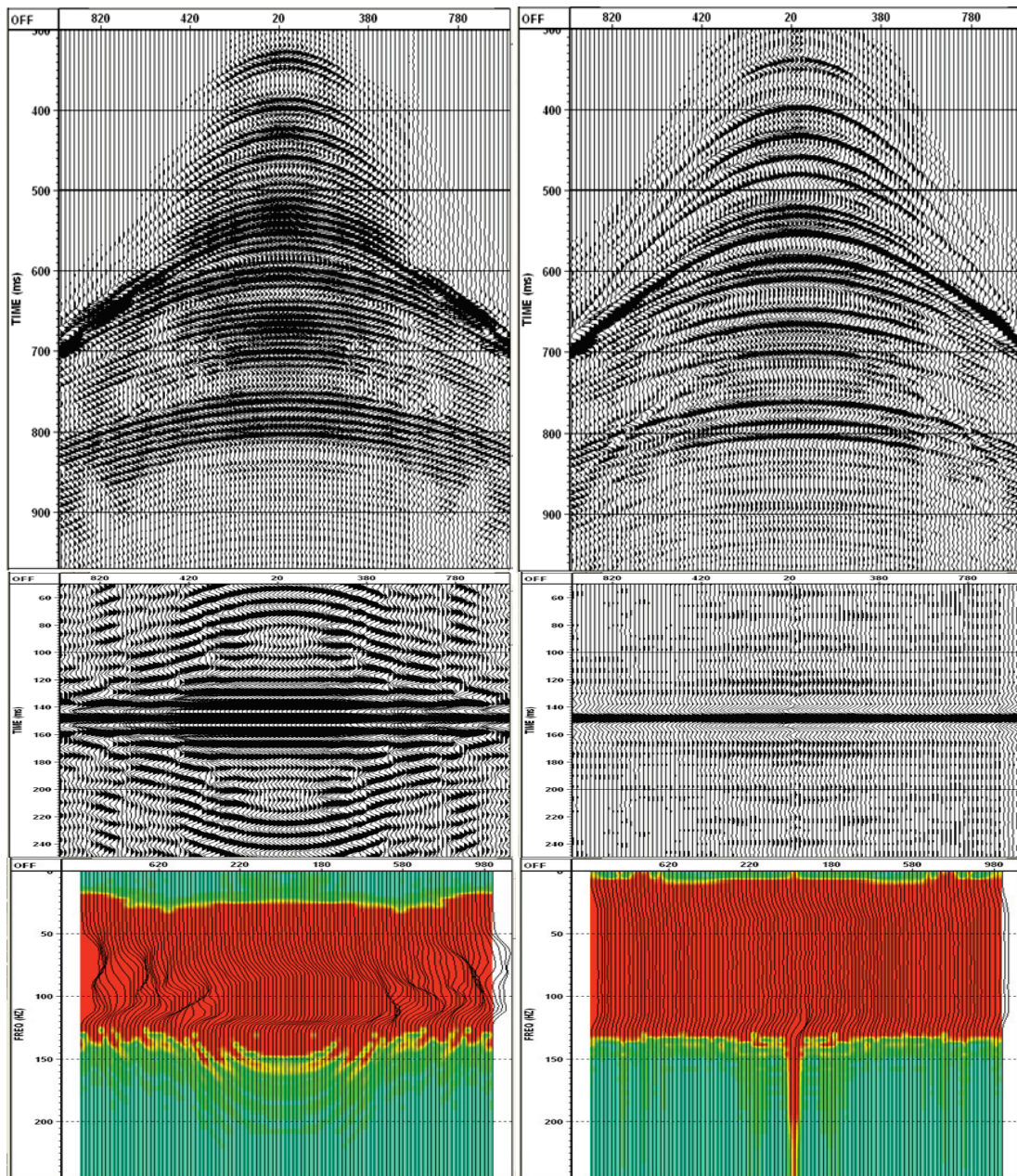


Figure 12. Comparison of vertical component of isotropic earth model before (left) & after (right) deconvolution. From top to bottom: gathers across source point at azimuth  $0^\circ$ ; autocorrelations of top gathers; amplitude spectrum plots of top gathers.

Velocity analysis was performed for both PP wave and PS waves. Since both earth models are laterally homogenous, a receiver line in x direction across the source point is considered to be a CRP gather for velocity analysis. By comparing NMO corrected gathers, velocity functions converted from velocities input for seismic modeling were adopted. Hyperbolic NMO is also found to be inadequate (Figure 13c and Figure 13f), thus  $\eta$  parameters were also picked for 4<sup>th</sup> order NMO (Figure 13a and Figure 13d). By applying 4<sup>th</sup> order NMO correction, far-offset events are also well flattened (Figure 13b and Figure 13e).

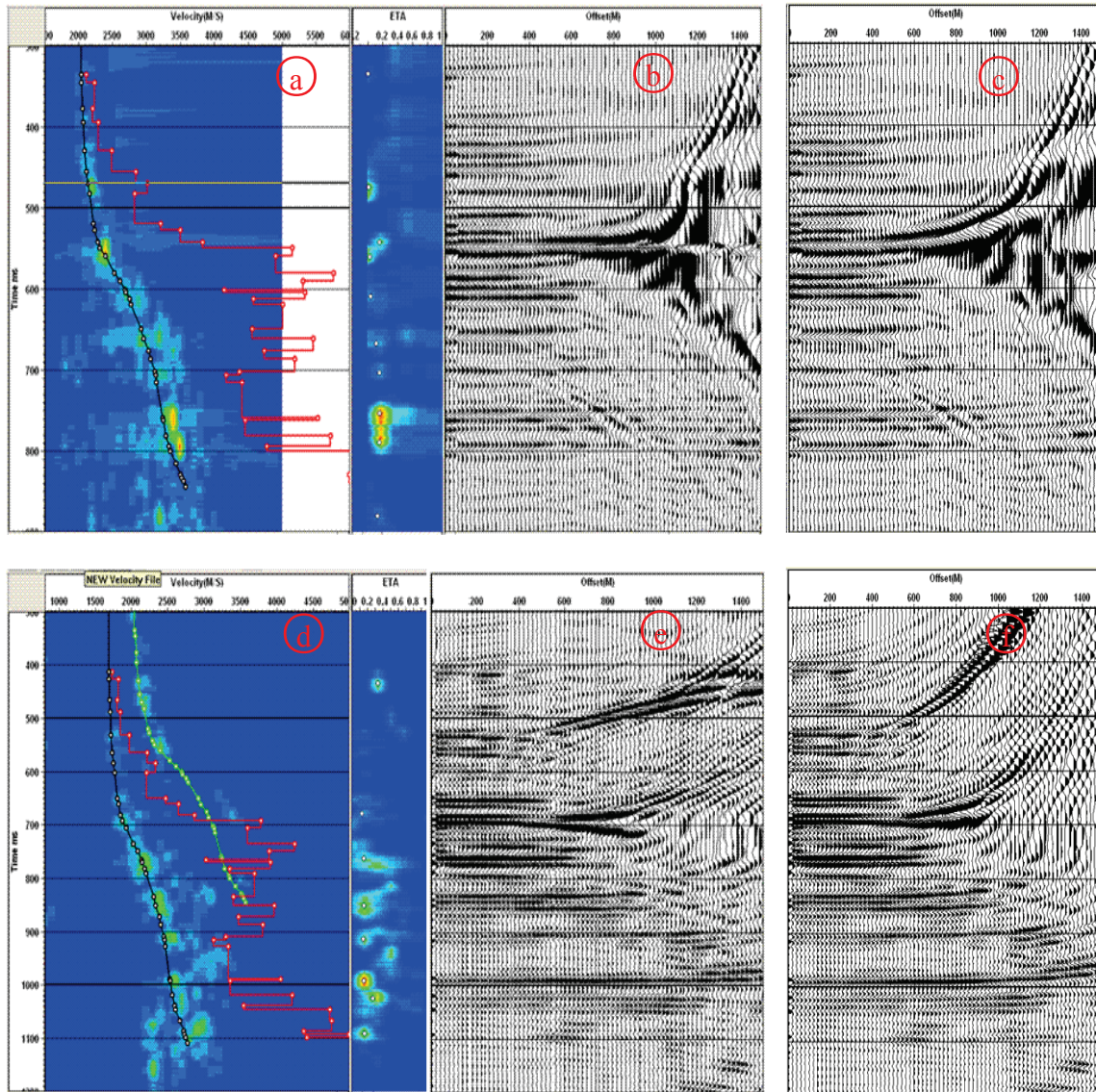


Figure 13. Velocity analysis for PP (top) and PS (bottom) data. From left to right: velocity spectrum, eta for 4<sup>th</sup> order moveout correction, 4<sup>th</sup> order NMO corrected gather, hyperbolic NMO corrected gather. Black line in the spectrum is the RMS velocity, read line is interval velocity, the green line in (d) denotes the velocity picks of P wave from (a).

Figure 14 displays NMO corrected azimuth-offset gathers of the vertical component for the isotropic model and the corresponding FK spectrum. Some coherent noise can be found (Figure 14 left). By applying FK filter, the coherent noise is mostly attenuated (Figure 14 middle). The data was then sorted into azimuth-offset supergathers. Azimuth gathers were grouped by an azimuth increment of 6°. Within each azimuth supergather, offsets were also grouped by 40m panels. For seismic anisotropy analysis, the azimuth-offset supergathers were also sorted in offset-azimuth order (Figure 15, Figure 16, and Figure 17). For shear-wave splitting analysis, common azimuth supergathers were stacked. The vertical, radial and transverse components stack results are shown as Figure 20, Figure 21 and Figure 22.

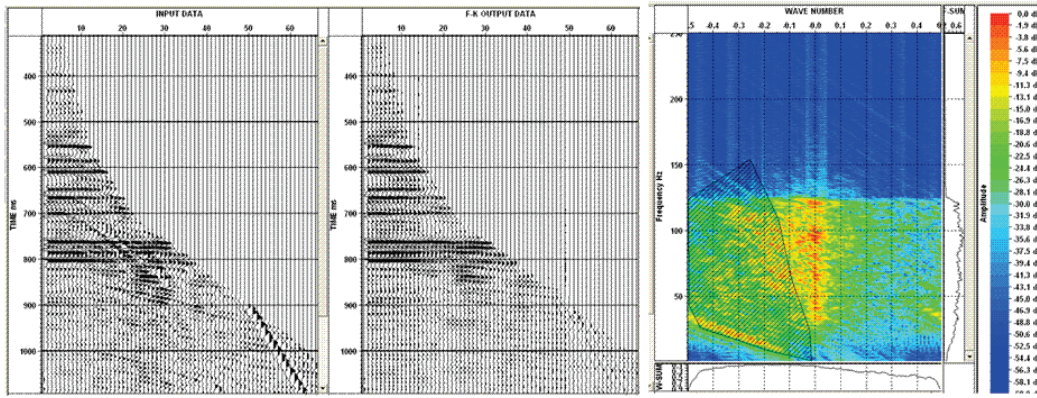


Figure 14. From left to right: vertical component azimuth gather of isotropic model before FK filtering; the same data after FK filtering, and FK spectrum & FK filter design.

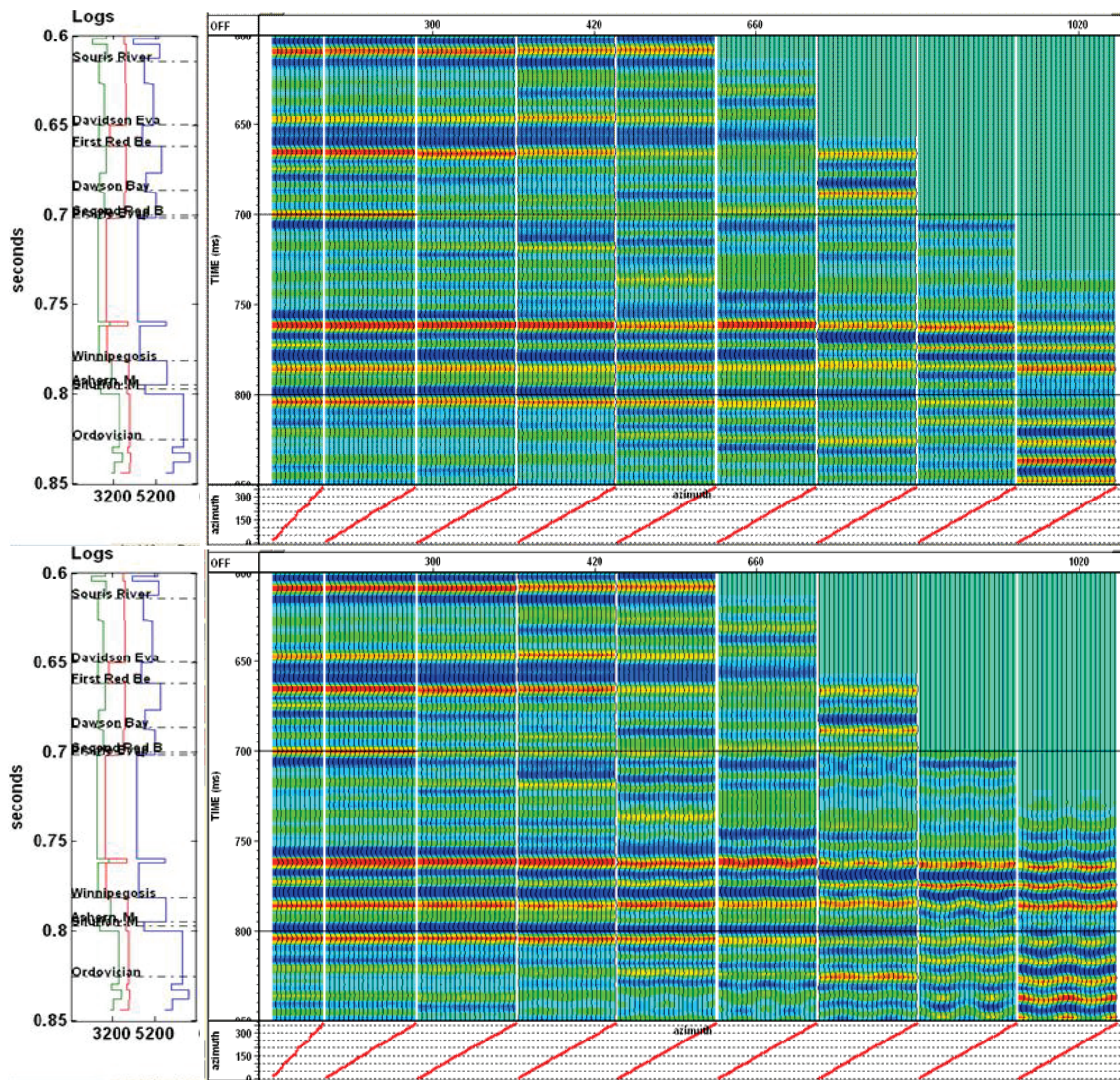


Figure 15. Well logs (Vp: blue; Vs: green; density: red) and offset-azimuth supergathers of vertical component for isotropic (top) and HTI (bottom) earth model. The red plots at the bottom are azimuth. Common-offset gathers are separated by space and offset increases to the right.

## RESULTS AND DISCUSSIONS

## Velocity anisotropy

The evidence of azimuth velocity anisotropy can be seen on the offset-azimuth supergathers of the vertical, radial and transverse components of the data (Figure 15, Figure 16 and Figure 17). On the vertical and radial component gathers of isotropic model, there is no sign of azimuthal velocity variation from near to far offset (the top gathers of Figure 15 and Figure 16). On the corresponding gathers of anisotropic model, since isotropic NMO correction was applied to the gathers, residual moveout was left on the NMO gathers. We can see the azimuthal variation of residual moveout on the gathers of anisotropic model below the reflection of the top of the Dawson Bay Formation. The variation range increases with offset, the largest variation is seen on the far offset. On the gathers of the transverse component, a similar phenomenon can also be observed (Figure 17).

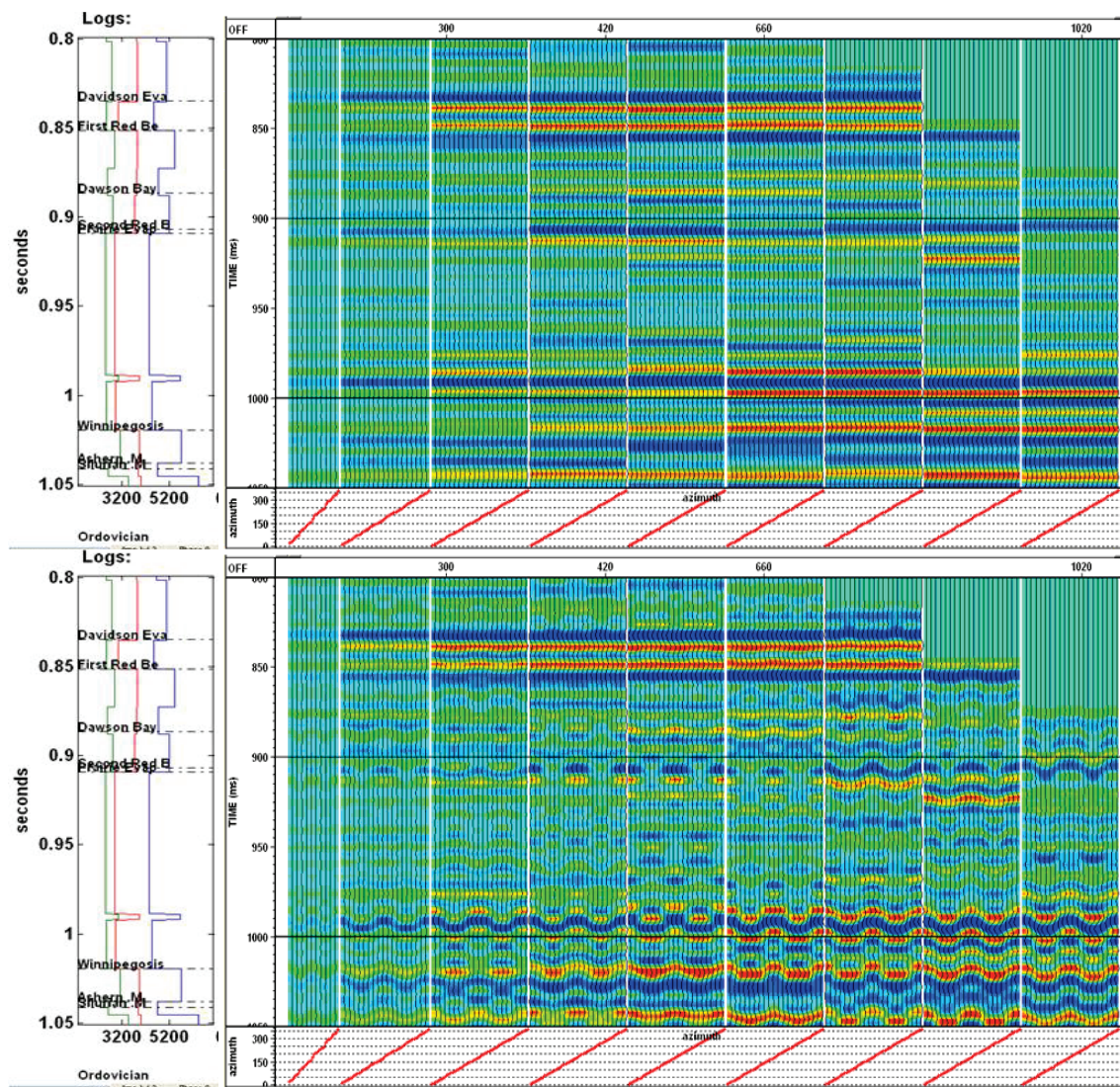


Figure 16. Well logs ( $V_p$ : blue;  $V_s$ : green; density: red) and offset-azimuth supergathers of radial component for isotropic (top) and HTI (bottom) earth model. The red plots at the bottom are azimuth. Common-offset gathers are separated by space and offset increases to the right.

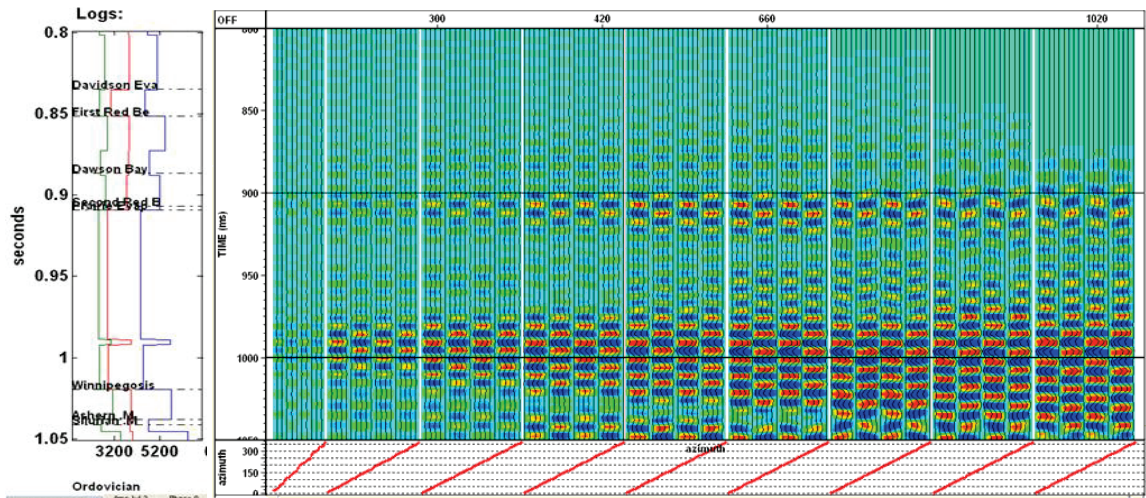


Figure 17. Well logs (Vp: blue; Vs: green; density: red) and offset-azimuth supergathers of transverse component for HTI earth model. The red plots at the bottom are azimuth.

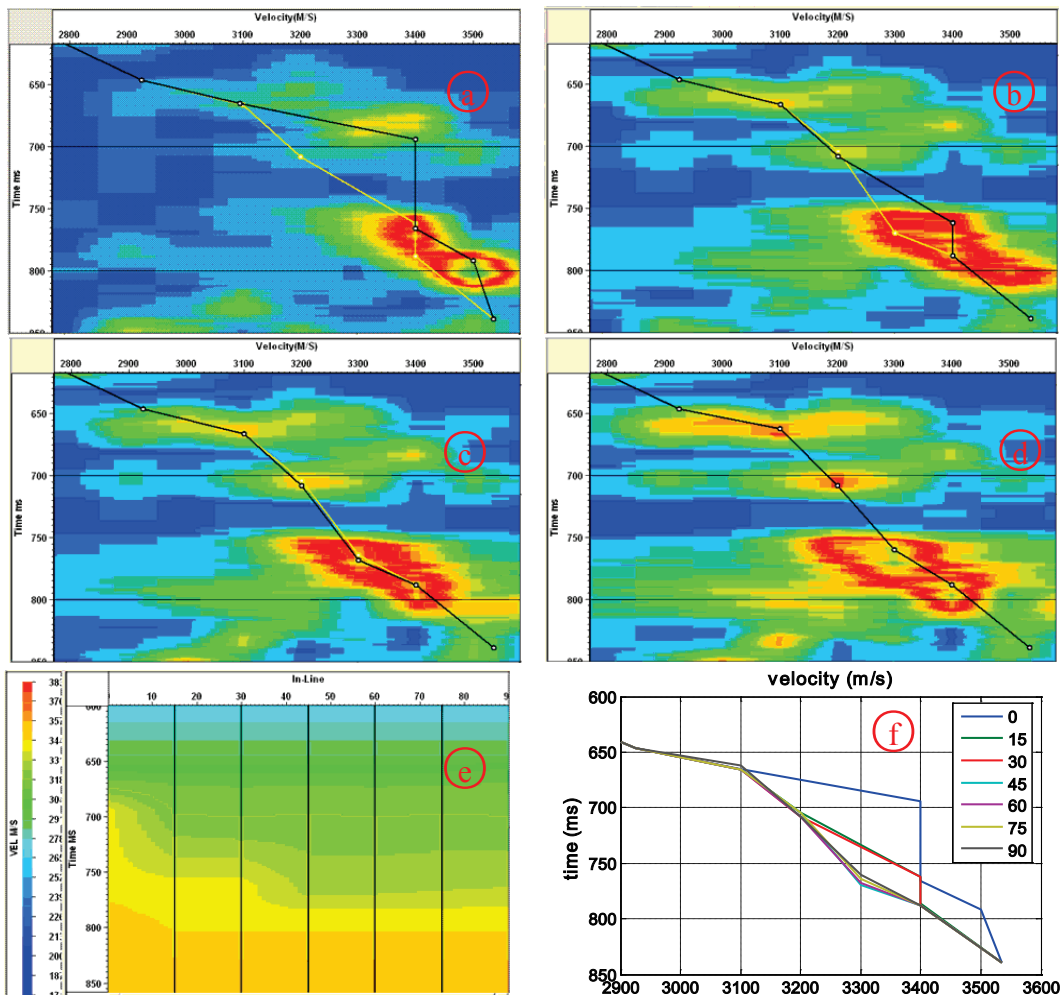


Figure 18. Vertical component velocity spectra (the black line denotes the velocity picks on the present spectrum, the yellow line is the picks on adjacent spectrum) of HTI model at azimuth 0° (a), 30° (b), 60° (c), and 90° (d), stack velocity section (e) and stack velocity plots at the seven azimuths (f).

Based on the azimuth super-gathers, azimuthal velocity analysis were carried out for both vertical and radial components for anisotropic model. Figure 18 show the velocity spectrum at four selected azimuths, velocity section and picked velocity plots of the vertical component focused on the cracked formation. The same plots for radial component are displayed as Figure 19.

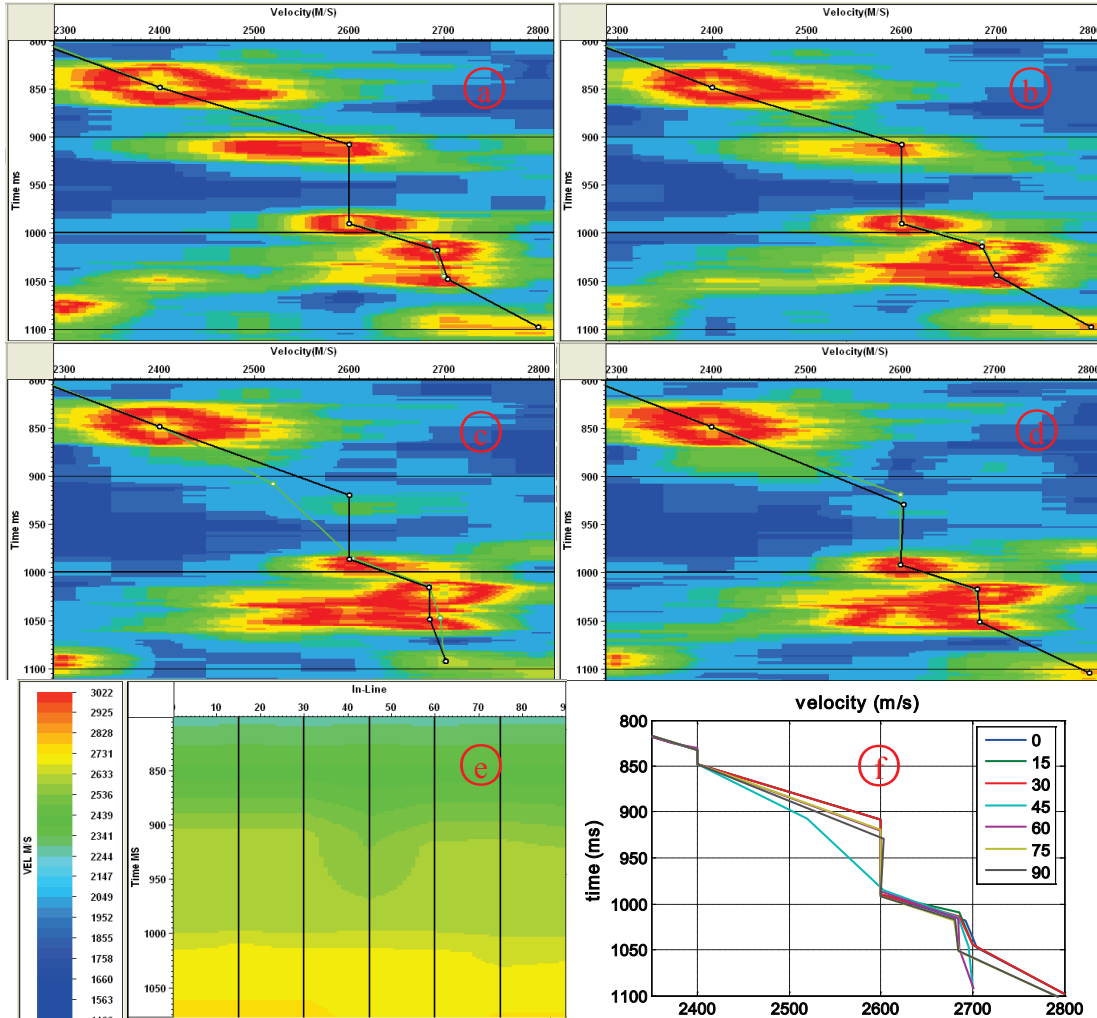


Figure 19. Radial component velocity spectra (the black line denotes the velocity picks on the present spectrum, the yellow line is the picks on adjacent spectrum.) of HTI model at azimuth 0° (a), 30° (b), 60° (c), and 90° (d), stack velocity section (e) and stack velocity plots at the seven azimuths (f).

From the azimuthal velocity spectrum, we can see the difference from the top of the First Red Bed Shale, about 665ms on vertical component, and 848ms on radial component. The stack energy peak locations of the base of the Dawson Bay (705ms on vertical component, 906ms on radial component) vary with azimuth. Smaller variation of the Shell Lake anhydrite (762ms on vertical component, 984ms on radial component) can also be seen on velocity spectrum. From the velocity map, we can see the velocity is constant above the top of the Dawson Bay. The maximum variation of stack velocity with azimuth exists at the bottom of the cracked Dawson Bay. The similar observation is also

visible on velocity plots of the six azimuths from 0 to 90 degree. For the P wave data, the maximum stacking velocity at the bottom of the Dawson Bay Formation is at azimuth 0°, which is parallel to the isotropy plane. The minimum stacking velocity of the base of the Dawson Bay Formation for the PS data is found to be at azimuth 45°.

### **Shear-wave splitting analysis**

Figure 20 and Figure 21 show the azimuth bin stack of vertical and radial components for both isotropic and HTI models. The stack results were also correlated to synthetic seismograms from well logs. The correlations between synthetic seismograms and azimuth bin stack are quite good for both vertical and radial components. The four events picked (from top to bottom) are the top of First Red Shale (Event 1), the top of Dawson Bay (Event 2), the base of Dawson Bay (Event 3), and the top of Shell Lake Anhydrite (Event 4). At the top of the First Red Bed Shale, stacks of isotropic and anisotropic models are quite consistent. Below Event 1, the reflections are coherent on stack results of isotropic model. On the stack results of anisotropic model, however, there are variations of amplitude and time. It is especially evident on the radial component. From the differences between stack results of isotropic and anisotropic models, we can see the minimum difference is at azimuth 0° and 180° (along crack plane direction) for both vertical and radial components, the maximum difference is at azimuth 90° and 270° (along crack normal direction). On the bin stack of transverse component (bottom of Figure 22), only the reflections below the top of the Dawson Bay can be seen and no sinusoidal shape reflections time variation is found. However, polarity flip happens across 0°, 90°, 180° and 270°. From the amplitude plots of the bottom two selected reflections Figure 23, the base of Dawson Bay and the top of Shell Lake Anhydrite, we can see that amplitude crosses 0 at these four azimuths. Within each quadrant, amplitude increases with azimuth for the first 45 degree then decreases.

Figure 22 shows the interpretation result of fast and slow shear-wave directions. Fast shear-wave S1 is along 0°-180° direction, which is consistent with the crack plane direction of the input model. Slow shear-wave orientation is along 90°-270° direction, the direction normal to the cracks of the input model.

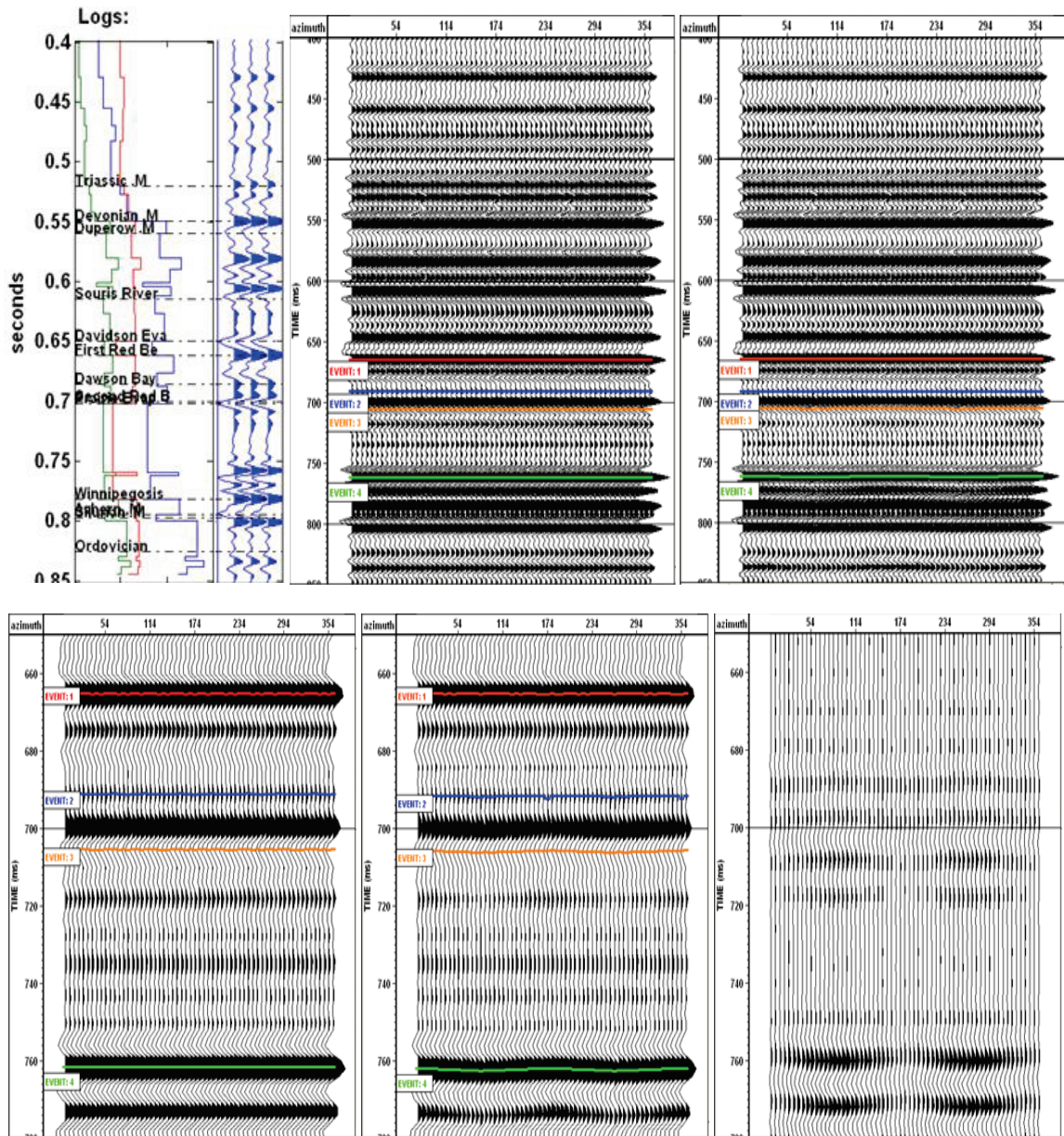


Figure 20. Top, from left to right: well logs, synthetic seismogram, azimuth bin stack of vertical component for isotropic earth model, and azimuth bin stack of vertical component for isotropic anisotropic earth model. Bottom, from left to right: azimuth bin stack of vertical component for isotropic (left) & anisotropic (middle) earth model, and their difference (right) focused on the cracked layer. The four events picked (from top to bottom) are the top of First Red Shale, the top of Dawson Bay, the base of Dawson Bay, and the top of Shell Lake Anhydrite.

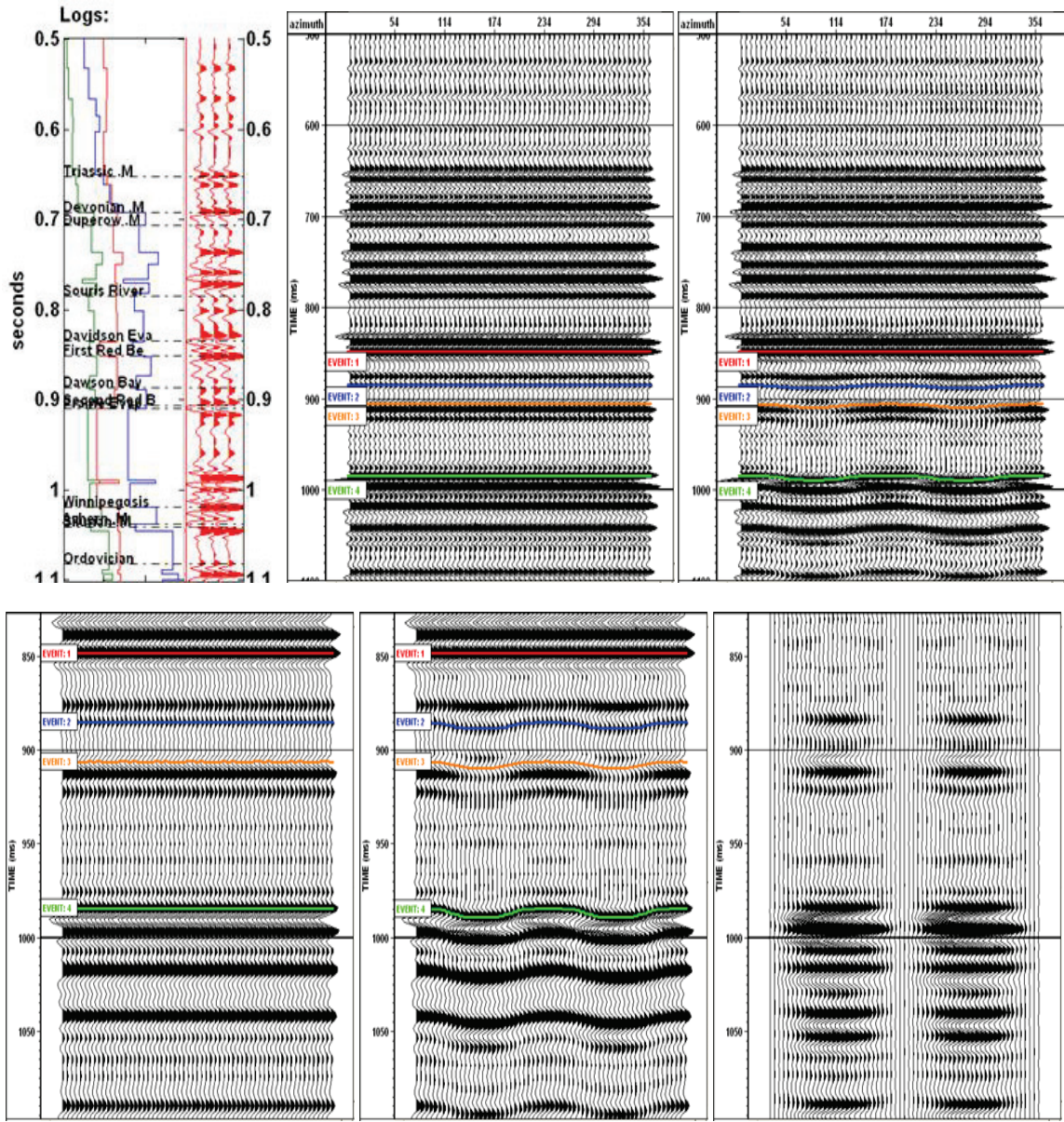


Figure 21. Top, from left to right: well logs, synthetic seismogram, azimuth bin stack of vertical component for isotropic earth model, and azimuth bin stack of vertical component for isotropic anisotropic earth model. Bottom, from left to right: azimuth bin stack of vertical component for isotropic (left) & anisotropic (middle) earth model, and their difference (right) focused on the cracked layer. The four events picked (from top to bottom) are the top of First Red Shale, the top of Dawson Bay, the base of Dawson Bay, and the top of Shell Lake Anhydrate.

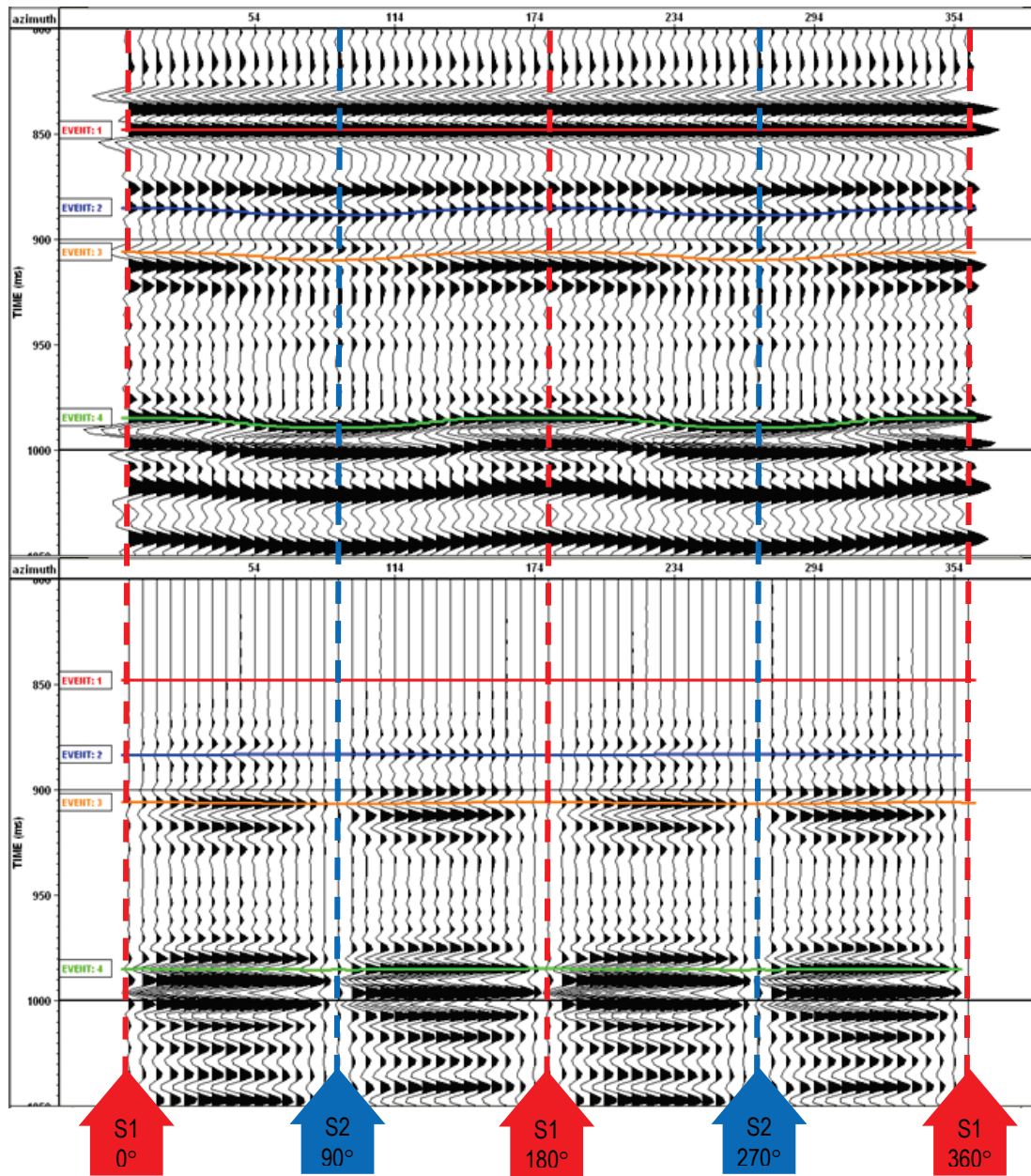


Figure 22. Radial (top) and transverse (bottom) components azimuth bin stack of cracked earth model. The red dashed lines show the fast shear-wave (S1) polarization direction and the blue dashed lines show the slow shear-wave (S2) polarization direction. The four events picked (from top to bottom) are the top of First Red Shale, the top of Dawson Bay, the base of Dawson Bay, and the top of Shell Lake Anhydrate.

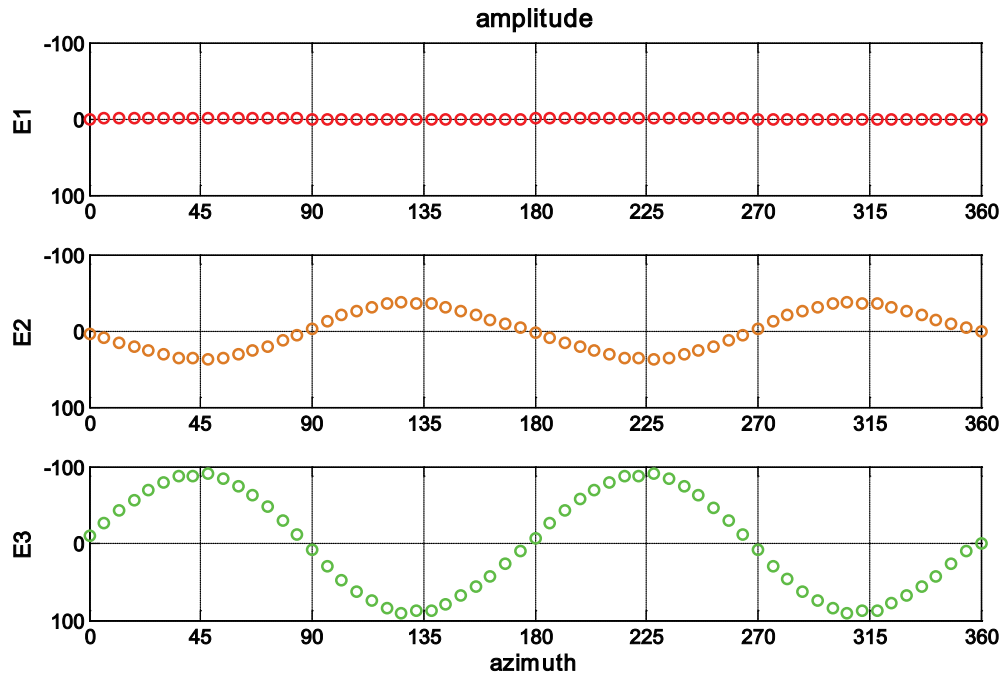


Figure 23. Amplitude plots of transverse component azimuth bin stack of the anisotropic model. The three events are the top of First Red Shale (E1), the base of Dawson Bay Formation (E2), and the top of Shell Lake Anhydrite (E3).

### Time-lapse attribute analysis

Time lapse attribute analysis were performed for time and amplitude of the three picked events mentioned before, the top of First Red Shale (E1), the base of Dawson Bay Formation (E2), and the top of Shell Lake Anhydrite (E3). Figure 24 displays the time and amplitude plots of the three events for vertical component of isotropic and HTI models together with the corresponding differences. At the top of the First Red Bed Shale (E1), since all the overlying strata of the two models are same and isotropic, there is almost no time shift from azimuth 0 to 360 degree. However, small amplitude difference, up to 3.2% increase, exists at the top of this layer. At the bottom of the Dawson Bay (E2), up to 0.75ms time delay and  $\pm 3.7\%$  amplitude change can be seen due to the fractures. Although all the formations underlying the Dawson Bay are totally the same for the two earth models and both isotropic, larger time delay (up to 1.1ms) and amplitude change (up to 12.2%) are found at deeper reflections, e.g., the top of Shell Lake Anhydrite (E3). The reason for the increases of time delay and amplitude change could be the incidence angle difference for E2 and E3 when P waves travel through the anisotropic layer.

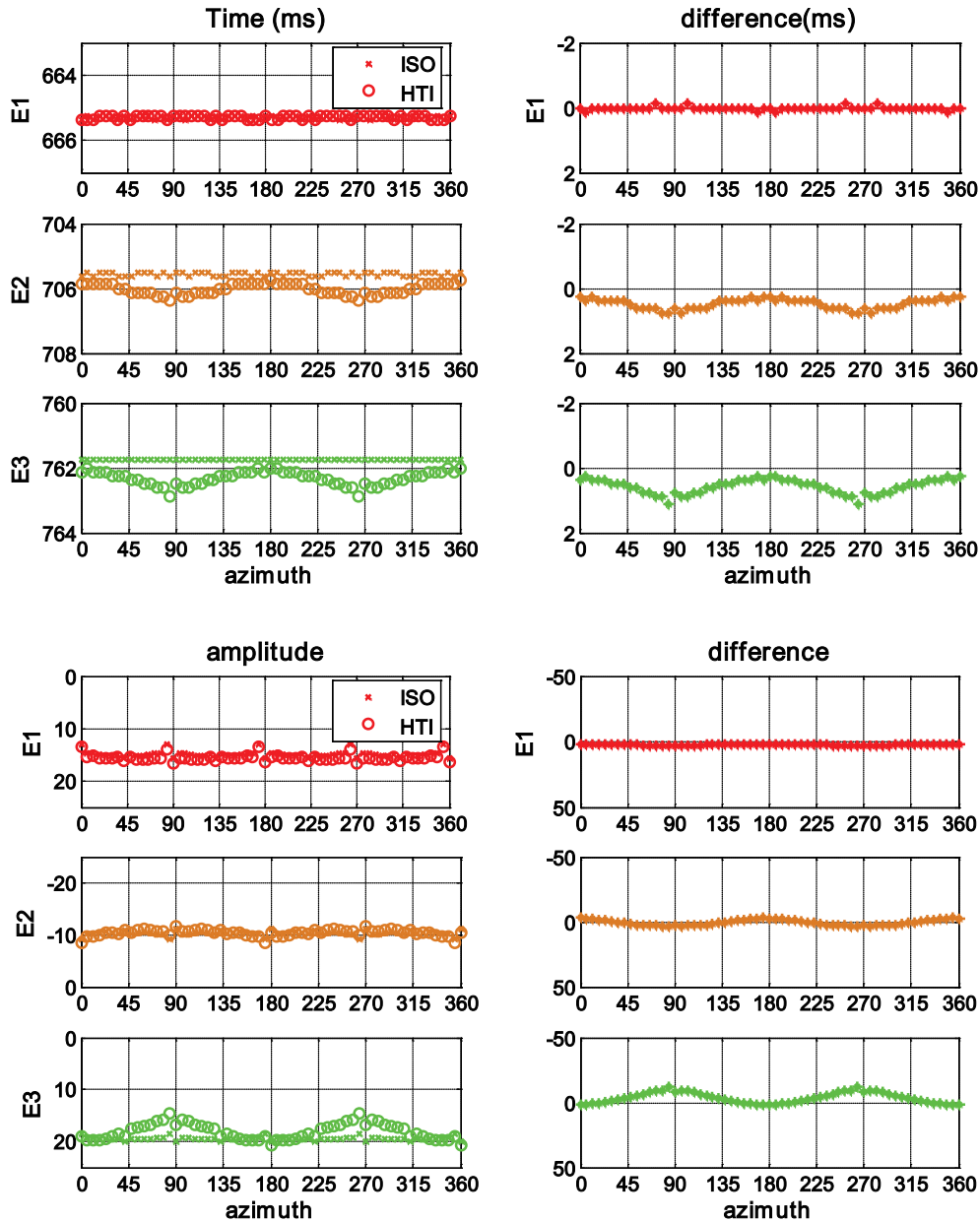


Figure 24. Time (upper) and amplitude (lower) plots of the three events on the vertical component azimuth bin stack for uncracked (denoted as ISO) and cracked (denoted as HTI) earth model. The amplitude differences are in percentage scale. The three events are the top of First Red Shale (E1), the base of Dawson Bay Formation (E2), and the top of Shell Lake Anhydrite (E3).

Figure 25 shows the time and amplitude plots of the three events on radial component of isotropic and anisotropic models together with corresponding differences. At the top of the First Red Bed Shale (E1), since all the overlying strata of the two models are same and isotropic, there is almost no time shift from azimuth 0 to 360 degree. Similarly, a small amplitude difference, up to 2.2% increase, can also be seen at the top of the anisotropic layer on radial component. At the bottom of the Dawson Bay (E2), we can see a larger time delay (up to 3.75ms) and amplitude change (up to 46% decrease) compared with vertical component. As seen for the vertical component, although all the

formations underlying the Dawson Bay are totally the same for the two earth models and both are isotropic, an increasing time delay (up to 4.9ms) is found at deeper reflections, e.g., the top of Shell Lake anhydrite (E3), and the amplitude change is up to 30%. The reason should be similar as what we observed on vertical component.

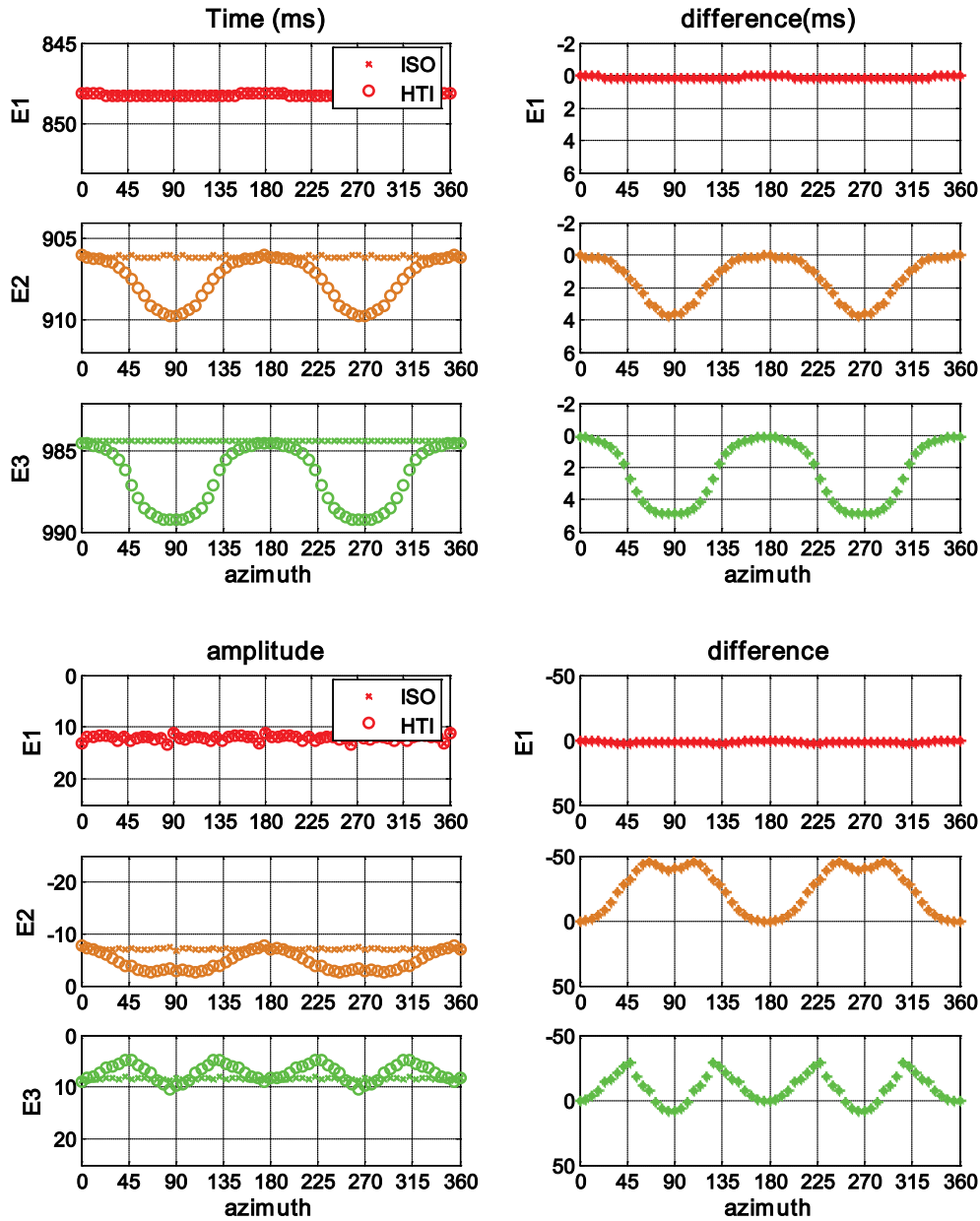


Figure 25. Time (upper) and amplitude (lower) plots of the three events on radial component azimuth bin stack for uncracked (denoted as ISO) and cracked (denoted as HTI) earth model. The amplitude differences are in percentage scale. The three events are the top of First Red Shale (E1), the base of Dawson Bay Formation (E2), and the top of the Shell Lake Anhydrite (E3).

**Discussion**

From the previous analysis, we can see that the anisotropy caused by vertically aligned cracks in the Dawson Bay Formation is evident on PP and PS data. From the offset-

azimuth gathers, residual moveout can be clearly seen since only isotropic NMO is applied on the data of HTI models. We can see the proof of anisotropy, on the other side, the time shift and amplitude difference might not be the same if NMO is accurately corrected by considering anisotropy effects.

However, vertically aligned cracks in the 40m Dawson Bay Formation can be detected by 3C seismic data. The time-shift and amplitude changes are significant, especially for radial-component data. The crack orientation can also be determined by the shear-wave polarization. Thus multi-component seismic data may be an effective way to map and monitor the crack in the Dawson Bay for potash mining.

## CONCLUSION

This report presents the processing and interpretation of seismic modeling data of the earth models generated based on well logs in a potash mining area of western Canada. The goal of the work is to study the evidence of azimuth seismic anisotropy, shear-wave splitting and time-lapse seismic signals caused by HTI anisotropy from vertically aligned cracks in the Dawson Bay Formation. The results show that seismic velocity anisotropy can be detected by both vertical and horizontal components of the HTI earth model, it is especially evident on radial component. Shear-wave splitting is distinct and the crack orientation determined from the polarization of fast and slow shear waves is consistent with the input model. The time-shift and amplitude changes due to anisotropic layer are also apparent on both vertical and radial component data. The time-shift on radial data is up to 5ms at the top of Shell Lake anhydrite, and the amplitude change is up to 46% at the base of Dawson Bay.

Combined with the correlation results of well and surface seismic data in the previous study, this suggests that multi-component seismic data could be interpretable in this potash area of western Canada. This also suggests that by searching for seismic anisotropy, shear-wave splitting on the multi-component seismic data or by looking for changes in repeated seismic surveys, we may be able to detect/monitor cracks and crack direction in the Dawson Bay and similar intervals.

## ACKNOWLEDGEMENTS

We thank James E. Gaiser of GX Technology for helping with the numerical modeling data. The seismic data processing is done by VISTA of GEDCO, we thank Carlos Montaña for help with the VISTA processing software. The support by the sponsors of the CREWES project is gratefully appreciated.

## REFERENCE

- Fuzesy, L.M., 1982, Petrology of potash ore in the Esterhazy Member of the Middle Devonian Prairie Evaporite in southeastern Saskatchewan, Proceedings of the Fourth International Williston Basin Symposium, 67-73.
- Gray, D., Schmidt, D., and Nagarajappa, N., et. al, 2008. An azimuthal-AVO-compliant 3D land seismic processing flow: 2009 CSEG Annual Convention, Expanded Abstracts.
- Stewart, R.R., and Gaiser, J.E., 2007. Application and interpretation of converted-waves, course notes: SEG Continuing Education.

- Van Dok, R., Gaiser, J., and Markert, J., 2001. Processing PS-wave data from a 3-D/3-C land survey for fracture characterization: EAGE 63<sup>rd</sup> Conf. and Tech. Exhibit., Expanded Abstract.
- Zhang, Z., and Stewart, R.R., 2008. Seismic detection of cracks in carbonates associated with potash mining: 2009 CSEG Annual Convention, Expanded Abstracts.